https://doi.org/10.5194/acp-2022-498
Preprint. Discussion started: 26 August 2022

An intercomparison study of four different techniques for measuring the chemical composition of nanoparticles

Lucía Caudillo[1], Mihnea Surdu[2], Brandon Lopez[3], Mingyi Wang[3,4], Markus Thoma[1], Steffen Bräkling[5], Angela Buchholz[6], Mario Simon[1], Andrea C. Wagner[1], Tatjana Müller[1,7], Manuel Granzin[1], Martin Heinritzi[1], Antonio Amorim[8], David M. Bell[2], Zoé Brasseur[9], Lubna Dada[2], Jonathan Duplissy[9,10], Henning Finkenzeller[11], Xu-Cheng He[9], Houssni Lamkaddam[2], Naser G. A. Mahfouz[3], Vladimir Makhmutov[12,13], Hanna E. Manninen[14], Guillaume Marie[1], Ruby Marten[2], Roy L. Mauldin[15,3], Bernhard Mentler[16], Antti Onnela[14], Tuukka Petäjä[9], Joschka Pfeifer[1,14], Maxim Philippov[12], Ana A. Piedehierro[17], Birte Rörup[9], Wiebke Scholz[16], Jiali Shen[9], Dominik Stolzenburg[9], Christian Tauber[18], Ping Tian[19], António Tomé[20], Nsikanabasi Silas Umo[21], Dongyu S. Wang[2], Yonghong Wang[9], Stefan K. Weber[1,14], André Welti[17], Marcel Zauner-Wieczorek[1], Urs Baltensperger[2], Richard C. Flagan[4], Armin Hansel[16,22], Jasper Kirkby[1,14], Markku Kulmala[9,10,23], Katrianne Lehtipalo[9,17], Douglas R. Worsnop[9,24], Imad El Haddad[2], Neil M. Donahue[3], Alexander L. Vogel[1], Andreas Kürten[1], Joachim Curtius[1].

[1]Institute for Atmospheric and Environmental Sciences, Goethe University Frankfurt, Frankfurt am Main, 60438, Germany
[2]Laboratory of Atmospheric Chemistry, Paul Scherrer Institute, 5232 Villigen, Switzerland
[3]Center for Atmospheric Particle Studies, Carnegie Mellon University, Pittsburgh, PA 15213, USA
[4]Division of Chemistry and Chemical Engineering, California Institute of Technology, Pasadena, CA 91125, USA
[5]TOFWERK AG, Thun, 3600, Switzerland
[6]Department of Applied Physics, University of Eastern Finland, Kuopio, Finland
[7]Atmospheric Chemistry Department, Max Planck Institute for Chemistry, 55128 Mainz, Germany
[8]CENTRA and Faculdade de Ciências da Universidade de Lisboa, Campo Grande 1749–016, Lisboa, Portugal
[9]Institute for Atmospheric and Earth System Research (INAR) / Physics, Faculty of Science, University of Helsinki, 00014 Helsinki, Finland
[10]Helsinki Institute of Physics, University of Helsinki, 00014 Helsinki, Finland
[11]Department of Chemistry & CIRES, University of Colorado Boulder, Boulder, CO, 80309-0215, USA
[12]Lebedev Physical Institute, Russian Academy of Sciences, 119991, Moscow, Russia
[13]Moscow Institute of Physics and Technology, Moscow, 117303, Russia
[14]CERN, 1211 Geneva, Switzerland
[15]Department of Atmospheric and Oceanic Sciences, University of Colorado Boulder, Boulder, CO 80309, USA
[16]Institute for Ion and Applied Physics, University of Innsbruck, 6020 Innsbruck, Austria
[17]Finnish Meteorological Institute, 00560 Helsinki, Finland
[18]Faculty of Physics, University of Vienna, 1090 Vienna, Austria
[19]Beijing Weather Modification Office, China
[20]IDL, Universidade da Beira Interior, R. Marquês de Ávila e Bolama, Covilhã, 6201-001, Portugal
[21]Institute of Meteorology and Climate Research, Karlsruhe Institute of Technology, Karlsruhe, Germany
[22]Ionicon Analytik GmbH, 6020 Innsbruck, Austria
[23]Aerosol and Haze Laboratory, Beijing Advanced Innovation Center for Soft Matter Science and Engineering, Beijing University of Chemical Technology, Beijing, 100029, P.R. China
[24]Aerodyne Research, Billerica, MA 01821 USA

Correspondence to: Lucía Caudillo (lucia.caudillo@iau.uni-frankfurt.de) and Joachim Curtius (curtius@iau.uni-frankfurt.de)

Abstract.

Currently, the complete chemical characterization of nanoparticles (<100 nm) represents an analytical challenge, since these particles are abundant in number but have negligible mass. Several methods for particle-phase characterization have been recently developed to better detect and infer more accurately the sources and fates of ultra-fine particles, but a detailed comparison of different approaches is missing. Here we report on the chemical composition of secondary organic aerosol (SOA) nanoparticles from experimental studies of α-pinene ozonolysis at -50 ºC, -30 ºC, and -10 ºC, and inter-compare the results measured by different techniques. The experiments were performed at the Cosmics Leaving OUtdoor Droplets (CLOUD) chamber at the European Organization for Nuclear Research (CERN). The chemical composition was measured simultaneously by four different techniques: 1) Thermal Desorption-Differential Mobility Analyzer (TD-DMA) coupled to a NO_3^- chemical ionization-atmospheric-pressure-interface-time-of-flight (CI-APi-TOF) mass spectrometer, 2) Filter Inlet for Gases and AEROsols (FIGAERO) coupled to an I^- high-resolution time-of-flight chemical-ionization mass spectrometer (HRToF-CIMS), 3) Extractive Electrospray Na^+ Ionization time-of-flight mass spectrometer (EESI-TOF), and 4) Offline analysis of filters (FILTER) using Ultra-high-performance liquid chromatography (UHPLC) and heated electrospray ionization (HESI) coupled to an Orbitrap high-resolution mass spectrometer (HRMS). Intercomparison was performed by contrasting the observed chemical composition as a function of oxidation state and carbon number, by calculating the volatility and comparing the fraction of volatility classes, and by comparing the thermal desorption behavior (for the thermal desorption techniques: TD-DMA and FIGAERO) and performing positive matrix factorization (PMF) analysis for the thermograms. We found that the methods generally agree on the most important compounds that are found in the nanoparticles. However, they do see different parts of the organic spectrum. We suggest potential explanations for these differences: thermal decomposition, aging, sampling artifacts, etc. We applied PMF analysis and found insights of thermal decomposition in the TD-DMA and the FIGAERO.

1 Introduction

So far there is no well-established instrument and technique to measure the complete chemical composition of ultrafine (< 100 nm) Secondary Organic Aerosol (SOA) particles. However, several analytical techniques have recently been developed in order to better advance our understanding on their chemistry. Techniques that are capable of measuring sub-30 nm particles include the Volatile Aerosol Component Analyzer (VACA) (Curtius et al., 1998), the Thermal Desorption Chemical Ionization Mass Spectrometry (TDCIMS) (Voisin et al., 2003), the Nano Aerosol Mass Spectrometer (NAMS) (Wang et al., 2006), the Aerosol time-of-flight mass spectrometer (Laitinen et al., 2009), the inlet for the size-resolved collection of aerosols (Phares and Collier, 2010), the Chemical Analyzer for Charged Ultrafine Particles (CAChUP) (Gonser and Held, 2013), the Electrostatic Precipitation-Electrospray Ionization Mass Spectrometry (EP-ESI-MS) (He et al., 2015), the Droplet Assisted Inlet Ionization (DAII) (Horan et al., 2017), and the Online Aerosol Chemical Characterization by Extractive Electrospray Ionization−Ultrahigh-Resolution Mass Spectrometer (EESI-Orbitrap) (Lee et al., 2020). Single-particle analysis by mass spectrometry methods based on aerodynamics, light scattering and laser desorption ionization are suitable for particles with larger sizes. These methods include for example, the Aerosol Mass Spectrometer (AMS) described in Jayne et al. (2000), and the suite of single particle methods described in the review by Bzdek et al. (2012). The detection of particles with $d < 100$ nm using these techniques becomes difficult, because the scattering efficiency decreases when the particle diameter becomes smaller.

Using the Cosmics Leaving OUtdoor Droplets (CLOUD) chamber at the European Organization for Nuclear Research (CERN), we used simultaneously four different techniques for measuring the chemical composition of ultrafine particles and inter-compare the results.

1. Thermal Desorption-Differential Mobility Analyzer (TD-DMA) coupled to a NO_3^- chemical ionization-atmospheric-pressure-interface-time-of-flight (CI-APi-TOF) mass spectrometer (Wagner et al., 2018);
2. Filter Inlet for Gases and AEROsols (FIGAERO) coupled to an I^- high-resolution time-of-flight chemical-ionization mass spectrometer (HRToF-CIMS) (Lopez-Hilfiker et al., 2014) ;
3. Extractive Electrospray Na^+ Ionization time-of-flight mass spectrometer (EESI-TOF) (Lopez-Hilfiker et al., 2019); and,
4. Offline analysis of filters (FILTER) using Ultra-high-performance liquid chromatography (UHPLC) and heated electrospray ionization (HESI) coupled to an Orbitrap high-resolution mass spectrometer (HRMS) (Ungeheuer et al., 2021).

None of the techniques presented in this work represents the perfect instrument. In fact, a perfect instrument would be the one that is able to measure quantitatively all the hundreds of organic compounds that are present in the newly formed particles, and identify the molecular structures (including their isomeric and spatial configuration) at high resolution and in real time. Such an ideal instrument does not exist; and at present a combination of techniques is required for a more complete characterization of SOA (Hallquist et al., 2009).

In order to compare the techniques mentioned above and to gain insights into their limitations (e.g., due to decomposition during evaporation, different ionization techniques, etc.), we performed α-pinene ozonolysis experiments at -50 ºC, -30 ºC and -10 ºC. For the experiments at -50 °C and -30 °C TD-DMA, FIGAERO and EESI-TOF were inter-compared while for the experiment at -10 ºC FILTER, FIGAERO and, EESI-TOF were inter-compared. We carried out the in-depth inter-comparison by a) comparing the observed composition as a function of oxidation state and carbon number, b) calculating the volatility and comparing the fraction of ultralow-volatility (ULVOC), extremely low-volatility (ELVOC), low-volatility (LVOC), semi-volatile (SVOC), and intermediate-volatility (IVOC) organic compounds, and c) comparing the thermograms (for the thermal desorption techniques: TD-DMA and FIGAERO), and by performing positive matrix factorization (PMF) analysis to the thermograms.

Because the four techniques provide chemical composition, and more specifically the carbon, hydrogen and oxygen content (CHO), we determined the carbon oxidation state (OSc), which is a metric for the degree of the oxidation of organic species in the atmosphere (Kroll et al., 2011). It is calculated based on the ratios O:C and H:C and is useful to describe organic mixtures upon oxidation processes. In addition, we calculated the volatility (as introduced by Donahue et al. (2011) and modified by Stolzenburg et al. (2018)), and determined to which volatility classes the detected compounds belong. Regarding the thermal desorption methods (TD-DMA and FIGAERO) we investigated the thermal behavior of the detected species. Both instruments collect particles before transferring them to the gas-phase. When a temperature ramp is applied, the species that are adsorbed on the surface gradually desorb (as represented on a thermogram). In order to evaluate whether the thermal desorption methods lead to significant decomposition during evaporation, we applied a method called positive matrix factorization (PMF) (Paatero and Tapper, 1994; Buchholz et al., 2020), in which a dataset matrix is expressed in terms of the sum of factors matrices and a residual matrix. Lastly, we present an overview on the advantages and disadvantages for the different methods. All methods presented here agreed on the most dominant compounds that are found in the nanoparticles. Nevertheless, they do see different parts of the organic spectrum. Therefore, the techniques are complementary. The four techniques described in this work are feasible for measuring SOA and represent an important analytical development.

2. Methods

2.1 Experimental approach

2.1.1 The CLOUD chamber experiment

We conducted experiments in the CLOUD chamber at CERN to study pure biogenic new particle formation (NPF), without the presence of nitrogen oxides (NOx). The CLOUD chamber is a stainless-steel cylinder with a volume of 26.1 m^3 which has been extensively described by Kirkby et al. (2011) and Duplissy et al. (2016). To create the particles, NPF was induced by continuously adding α-pinene and ozone into the chamber. The monoterpene concentration was regulated by an evaporation source, in which dry nitrogen (N_2) passes through an evaporator containing liquid α-pinene at a precisely controlled temperature. Ozone was produced by exposing cryogenic O_2 to UV light and was introduced directly into the chamber via a separate line. The relative humidity was adjusted with a temperature-controlled Nafion humidifier using ultrapure Millipore water. All the precursor gases were homogenously mixed in the chamber by two magnetically driven Teflon fans placed at the top and at the bottom of the chamber. The temperature was kept constant by an insulated thermal housing, which surrounds the chamber. The α-pinene mixing ratio was measured by a proton transfer reaction time-of-flight (PTR-TOF) mass spectrometer (Graus et al., 2010; Breitenlechner et al., 2017), whereas ozone was measured by a TEI 49C ozone analyzer (Thermo Environmental Instruments). The experiments relevant for this work were performed at -50 ºC, -30 ºC, and -10 °C. The α-pinene mixing ratio ranged between 1 and 8 ppbv and ozone was approximately 100 ppbv. Figure S1 in the Supplement provides an overview of a representative experiment at -30 ºC.

Table 1 presents the most important features for the instruments used in this work. We categorize the techniques according to certain criteria: continuous or discontinuous operation mode, evaporation method, phase measured, ionization technique, reagent ion, target substances, occurrence of significant thermal decomposition and, whether the technique allows to perform size-resolved analysis of aerosol particles.

2.1.2 Thermal Desorption-Differential Mobility Analyzer (TD-DMA) coupled to a NO_3^- chemical ionization-atmospheric-pressure-interface-time-of-flight (CI-APi-TOF) mass spectrometer

The TD-DMA coupled to a NO_3^- CI-APi-TOF analyzes the chemical composition of nanoparticles in a semi-continuous mode of operation. The design and characterization have been reported by Wagner et al. (2018). This method allows gas-and particle-phase measurements using the same ionization technique. Individual results of gas-and particle-phase comparison of the same chemical system as in this study were reported in Caudillo et al. (2021). While the gas-phase measurement is taking place with the CI-APi-TOF mass spectrometer, the TD-DMA samples particles from the chamber. The particles are charged by an X-Ray source and then collected on a platinum/rhodium (90:10) filament by electrostatic precipitation. After a certain collection time (in this study ~ 4 hours), an electric current is applied to the filament, which causes its direct heating. We estimate based on the filament resistance, that the temperature gradually increased up to approximately 600 ºC in a period of ~ 1 minute (details of the heating curve will be discussed in Section 3.2).

The vapors that evaporate from the heated particles are carried by an N_2 flow to the nitrate CI-APi-TOF for chemical composition analysis. For chemical ionization of the vapors, nitrate reagent ions $(HNO_3)_n\,NO_3^-$ with n = 0-2 are created by a corona discharge (Kürten et al., 2011; Kürten et al., 2014). Some of the vapor molecules are ionized and subsequently detected by the APi-TOF mass spectrometer. A second heating cycle of the particle collecting filament is performed afterwards (without particle collection) in order to estimate the instrumental background due to the heating of the inlet line; this enables a more accurate particle signal estimation. Besides the particle and background estimations, a second heating up to ~ 600 ºC ensures that the filament is clean and avoids memory effects for the next measurement. With the nitrate ionization technique, sulfuric acid, iodic acid, methane sulfonic acid, and highly oxygenated molecules (HOMs) can be detected.

2.1.3 Filter Inlet for Gases and AEROsols (FIGAERO) coupled to an I^- high-resolution time-of-flight chemical-ionization mass spectrometer (HRToF-CIMS)

The Filter Inlet for Gases and AEROsols (FIGAERO) coupled to an I^- high-resolution time-of-flight chemical-ionization mass spectrometer (HRToF-CIMS) was first described by Lopez-Hilfiker et al. (2014) and optimized for CLOUD operation conditions by Wang et al. (2020). FIGAERO uses a multi-port to measure in alternation both gas-and particle-phase following the same general procedure as the TD-DMA/CI-APi-TOF. While the gas-phase is analyzed, particle collection takes place on a polytetrafluoroethylene (PTFE) filter, and after a certain collection time (in this study 15 minutes), the filter is automatically moved into the ion-molecule reactor and exposed to a pure N_2 gas flow. The N_2 flow is gradually heated to evaporate the particles by thermal desorption using a temperature-programmed heating curve. For the measurements reported in this study, the temperature was slowly ramped from room temperature up to 150 ºC in approximately 15 minutes. When the heating cycle ends a new collection starts, and the process repeats (an example of the heating curve is discussed in Section 3.2). The detection technique is based on iodide-molecule adduct ionization. Iodine ions I^-, I_3^- and $(H_2O)I^-$ are generated from a solution of methyl iodide (CH_3I) and a Po-210 ion source (Lee et al., 2014). With this soft ionization technique, the FIGAERO HRToF-CIMS can detect HOMs, organosulfates, and inorganic acids such as sulfuric acid and nitric acid.

2.1.4 Extractive electrospray Na^+ ionization time-of-flight mass spectrometer (EESI-TOF)

The Extractive electrospray ionization time-of-flight mass spectrometer (Lopez-Hilfiker et al., 2019) is a technique used for online particle-phase measurements without particle collection. This technique aims to provide the chemical composition of organic particles in real time. It is also possible to measure the gas-phase by using the dual configuration (Lee et al., 2022). In the beginning of the sampling process, the aerosol sample passes through the inlet line where a carbon denuder is located to remove the gas-phase molecules. The particles then collide with electrospray droplets and the soluble components are extracted and ionized. The EESI-TOF uses here an electrospray solution of pure water doped with 100 ppm NaI and is running in the positive ion mode. This enables the measurements of SOA species as adducts with Na^+. The electrospray droplets are evaporated as they pass through a heated stainless-steel capillary via the Coulomb explosion mechanism and the analytes are detected by a time-of-flight mass spectrometer. With this ionization method, various organic compounds that are relevant for atmospheric SOA particles can be analyzed, with the exception of species that are not oxygenated and organosulfates.

2.1.5 Offline analysis of filters (FILTER) using Ultra-high-performance liquid chromatography (UHPLC) and heated electrospray ionization (HESI) coupled to an Orbitrap high-resolution mass spectrometer (HRMS)

This procedure was optimized and described in detail by Ungeheuer et al. (2021). The method enhances the separation of organic compounds with high-resolution, and enables the determination of the accurate mass. The analysis consists mainly of four steps: sampling, extraction, separation, and detection.

First, the particles were collected from a flow of 5 l min^{-1} on a 47 mm diameter Emfab™ Filter (Pall Life Science, USA). After sampling, the filter was stored at -18 °C to avoid possible losses by evaporation. The filter was cut into small pieces (approximately 3 x 3 mm) and extracted two times in 0.2 ml solution (mixture of 90 % water and 10 % methanol) for 20 min. After each extraction step, the extract was filtered through a syringe filter (PTFE with a pore size of 0.2 µm). For chromatographic separation a gradient of ultrapure water (eluent A, Milli-Q Reference A+, Merck Millipore) and methanol (eluent B, Optima LC/MS Grade, Fisher Scientific) was applied. Both eluents were mixed with 0.1 % formic acid (v/v) for improved chromatographic performance. The injection volume was 5 µl, the flow rate was 400 µl min^{-1}, and the temperature was 40 °C. The gradient started with 1 % eluent B (0-0.5 min), increased linearly to 99 % B (0.5-14 min), stayed at 99 % B (14-16 min), backflushed in 1 min, and equilibrated in 3 min, resulting in a total run time of 20 min. Negative ionization mode was used for the detection, in which the molecular ions $[M-H]^-$ are produced by deprotonation. The ion source setting used for this purpose were: -3.5 kV spray voltage, 40 psi sheath gas, 8 arbitrary units auxiliary gas, and 262.5 °C capillary temperature. The scan range in full MS was 50-750 *m/z* with a mass resolving power of about 70k at *m/z* 200. For data-dependent MS^2 ($ddMS^2$) the resolution was 17.5k. Fragments were produced in a higher-energy collisional dissociation (HCD) cell with stepped collision energies of 15, 30, and 45 eV.

2.2 Data analysis

2.2.1 Data processing

TD-DMA, FIGAERO and EESI-TOF raw data was processed using IGOR Pro 7 (WaveMetrics, Inc., USA) and Tofware (Version 3.1.2, Aerodyne Inc., USA). The data from the offline method was processed with Compound Discoverer 3.2 (Thermo Fisher Scientific).

TD-DMA data was corrected by the mass-dependent transmission efficiency in the mass classifier (Heinritzi et al., 2016) and normalized by the nitrate reagent ions. FIGAERO raw data was averaged to 1 minute and normalized by the reagent ions. EESI-TOF raw signals were averaged to 10 seconds and normalized by the most abundant electrospray ion ($NaINa^+$). Additionally, for the comparison at -30 ºC and -50 ºC, EESI-TOF and FIGAERO data was averaged during the period where the TD-DMA collected particles. While for the comparison at -10 ºC, the average period corresponded to the time where the particles were collected with the FILTER for the offline analysis.
The postprocessing was done using MATLAB R2022a (MathWorks, Inc., USA).

2.2.2 Positive matrix factorization (PMF) analysis

One of the main questions we want to answer in this work is whether the thermal desorption methods (TD-DMA and FIGAERO) experience significant decomposition during the desorption process. To answer this question, we utilized positive matrix factorization (PMF) analysis. This method was originally described by Paatero and Tapper (1994) for analyzing time series of variable (e.g. mass spectra data) from ambient observations, and it was implemented by Buchholz et al. (2020) to thermal desorption data for identifying different processes during particle evaporation. We therefore applied the same procedure as Buchholz et al. (2020) to the TD-DMA and FIGAERO thermal desorption profiles (for the α-pinene oxidation experiment at -30 ºC and 20 % RH). For the analysis, we processed separately 1-second TD-DMA and 1-second FIGAERO thermograms. Since the FIGAERO measures in a semi-continuous mode, we chose a representative thermogram. Both TD-DMA and FIGAERO data sets were background subtracted. For the TD-DMA background, we used the second heating cycle that is performed immediately after the first heating (described in Section 2.1.2). For the FIGAERO background, we used a period where no significant particle load was present in the chamber (at the beginning of the experiment). We considered only the organic compounds and excluded the reagent ions for this analysis. We ran the PMF software using the CNerror scheme (based on the noise of each ion) and up to 10 different solutions. 4-factor TD-DMA and 6-factor FIGAERO solutions (discussed later in Section 3.2.1) were chosen as the most interpretable results by a) comparing the residuals and by looking at which solution captured the total signal and certain species the best (e.g., $C_8H_{12}O_4$), b) by finding an equilibrium between good reconstructed signal and physically interpretable results. This means, that for the solutions presented here, likely a higher number of factors improve the residuals, nevertheless, we chose the solution with the smallest number of factors that can still provide realistic information.

3. Results and discussion

3.1 Chemical composition comparison

Figure 1 shows the OS_C, calculated as $OS_C = 2 \times O{:}C - H{:}C$ (an approximation stated by Kroll et al. (2011)) against the number of carbon atoms for α-pinene oxidation products in the particle-phase at -30 ºC and 20 % RH as measured by three different techniques: TD-DMA, FIGAERO, and EESI-TOF. For all techniques, the highest intensities correspond to compounds with 10 carbon atoms (C_{10}) for which the oxidation state varies between 0.5 and -1.5 depending on the measurement technique. Compounds with more than 10 carbon atoms were also detectable by the TD-DMA, FIGAERO and EESI-TOF. The TD-DMA and FIGAERO detected also compounds with less than 5 carbon atoms and $OS_C > 0$ which, in contrast, are not detected by the EESI-TOF (this feature will be discussed in Section 3.2.1). In order to simplify the comparison, we calculated the fraction of species containing less than 10 carbon atoms ($C_{<10}$), 10 carbon atoms (C_{10}), and more than 10 carbon atoms ($C_{>10}$), since this can provide an insight of the detected fraction of monomers and dimers for each technique (Figure 1d). Approximately 42 %, 32 %, and 23 % of the signals correspond to $C_{<10}$, 47 %, 65 % and, 53 % to C_{10} and, around 11 %, 3 %, and 24 % to $C_{>10}$ measured by the TD-DMA, FIGAERO and EESI-TOF, respectively. Figure S2 in the Supplement displays the results for the experiments at -50 ºC. In every case, C_{10} represents the highest fraction detected by all the techniques in this experiment. Nevertheless, we do see significant differences between the techniques for $C_{<10}$, C_{10}, and $C_{>10}$.

The chemical ionization utilized by the TD-DMA (nitrate, NO_3^-) is more sensitive towards highly oxygenated species, while the FIGAERO (iodide, I^-) detects intermediately oxygenated species with higher sensitivity. In Figures S3 and S4 in the Supplement, we present the results (number of oxygen atoms vs number of carbon atoms) at -30 ºC and -50 ºC, respectively. From the figures (S3 and S4) we observe that more oxygenated species contribute more to the total signal on TD-DMA than in FIGAERO, this observation is consistent with the sensitivity that one would expect according to the chemical ionization. The electrospray ionization (Na^+) for the EESI-TOF is usually more sensitive towards intermediate oxygenated species, even though in the results presented here, it seems to capture very well the whole spectrum.

Besides the reagent ion selectivity, several factors can explain the quantitative differences. For example, both the TD-DMA and FIGAERO detect a lower fraction of $C_{>10}$ (11 % and 3 % compared to 24 % for the EESI-TOF). The TD-DMA and FIGAERO techniques are based on thermal desorption, which may cause decomposition of thermally unstable compounds during evaporation (as discussed in more detail in Section 3.2.1). On the other hand, the resulting fractions of $C_{>10}$ can be influenced by the ionization method employed: chemical ionization and electrospray are soft techniques, for which one can expect little fragmentation. Thus, we presume that thermal decomposition during evaporation could be the most significant factor that explain these differences.

Figure 2 presents the results for the experiment conducted at -10 ºC (α-pinene oxidation products at 80 % RH) for particles collected on a FILTER (Fig. 2a) and later analyzed by the UHPLC-HESI-HRMS method, and as measured by the FIGAERO and EESI-TOF (Fig. 2b and 2c, respectively). Overall, fewer compounds are detected by UHPLC-HESI-HRMS than by FIGAERO and EESI-TOF. The highest intensities in Fig. 2a (FILTER) correspond to $C_8H_{12}O_4$, $C_9H_{14}O_4$, $C_{10}H_{16}O_{3\text{-}6}$, $C_{17}H_{26}O_8$, and $C_{19}H_{28}O_7$. Ions with the same formulas are also detected by the FIGAERO and EESI-TOF, but the contribution to the total signal differs. The results at -10 ºC (number of oxygen atoms vs umber of carbon atoms) are shown in Figure S5 in the Supplement. By applying the UHPLC-HESI-HRMS method, it is possible to distinguish between compounds with identical chemical formula (isomers). For the experiment reported here, two isomers for $C_8H_{12}O_4$, $C_{10}H_{16}O_3$, and $C_{10}H_{16}O_5$, as well as three isomers for $C_{10}H_{16}O_4$ and $C_{10}H_{16}O_6$ were detected. The detection of these isomers is enabled by the chromatographic separation (their interaction with a reversed-phase column results in different retention times and therefore makes the separation feasible). However, complementary experiments are needed to investigate the molecular structure. Furthermore, Figure 2d shows the contributions of the $C_{<10}$, C_{10} and $C_{>10}$ fractions to the total signal for the FILTER, FIGAERO and EESI-TOF. At -10 ºC, the fraction of compounds with more than 10 carbon atoms ($C_{>10}$) has the smallest contribution to the total signal (14 %, 5 % and, 24 % for the FILTER, FIGAERO and EESI-TOF, respectively). The fractions $C_{<10}$ and C_{10} do not seem to have a clear tendency, they both contribute substantially to the total signal in each technique.

3.1.1 Volatility classes

We calculated the volatilities of the detected particle-phase compounds and associated them with defined volatility classes. We used the parametrization introduced in Donahue et al. (2011) and modified by Stolzenburg et al. (2018). This approach has been also discussed in Simon et al. (2020), and Wang et al. (2020). The volatility was calculated from the number of carbon and oxygen atoms in the specific molecules, and it was first defined at 300 K. By using the Clausius–Clapeyron equation, the volatility was then shifted according to the corresponding experimental temperature. The evaporation enthalpy was approximated according to Donahue et al. (2011) and Epstein et al. (2009). Thereafter the volatility was associated with any of the following classes: ultralow-volatility (ULVOC), extremely low-volatility (ELVOC), low-volatility (LVOC), semi-volatile (SVOC), and intermediate-volatility (IVOC) organic compounds.

Figures 3 and 4 show the contribution of each volatility class to the total particle signal for the corresponding experiment and for each technique. The results at - 50 ºC are reported in the Figure S6 in the Supplement. For the experiment at -30 ºC (Fig. 3), LVOC constitute the higher fraction for the TD-DMA, FIGAERO and, EESI-TOF. EESI-TOF detects the highest fraction of ULVOC (~ 12 % compared to 6 %, and 2 % measured by TD-DMA and FIGAERO, respectively). An IVOC fraction (~ 8 %) is only detected by the EESI-TOF. At -10 ºC (Figure 4), semi-volatile organic compounds (SVOC) contribute the most to the total particle signal for the FILTER, FIGAERO and EESI-TOF. Very small fractions of ULVOC are also detected by all the techniques. The EESI-TOF detects a higher fraction of IVOC (20 %) than FILTER and FIGAERO (2 % and 4 %), respectively. Taking into account the particle load (~1-3 ug m^{-3}) and size of the particles (diameter < 100 nm), it is possible that a significant fraction of IVOC measured by the EESI-TOF results from measurement artefacts, as seen in previous studies using EESI (Surdu et al., 2021). Several reasons (or a combination of them) can explain this feature: a) the Na^+ ionization technique may be more sensitive to lower oxygenated organic compounds than the I^- or NO_3^- techniques; b) likely, some amount of the gas-phase broke through the charcoal denuder (although its efficiency is > 99 %) and reached the detector. Lee et al. (2021a) reported that the EESI-TOF is more sensitive toward gas-phase analytes as compared to their particle-phase counterparts and, c) it can possibly occur some ion-induced fragmentation.

Overall, we observed that the contribution of the lowest volatility classes (ULVOC, ELVOC and LVOC) increases as the temperature decrease. This observation reflects two opposing temperature effects, as discussed in Ye et al. (2019) based on FIGAERO results: autoxidation and thus the extent of oxidation is reduced at low temperature, but any given compound is much less volatile at low temperature because of the strong dependency between saturation concentration and temperature.

3.2 Thermal desorption methods: TD-DMA and FIGAERO

Figure 5 shows the thermograms obtained by the FIGAERO and TD-DMA for the species $C_8H_{12}O_4$, $C_9H_{14}O_4$ and $C_{10}H_{16}O_6$ detected in the α-pinene ozonolysis experiment at -30 ºC. In Fig. 5a, c and e, we show a representative thermal desorption profile measured by FIGAERO. During the desorption time (~ 15 minutes), the normalized intensity of $C_9H_{14}O_4$ and $C_{10}H_{16}O_6$ first increased, reached a maximum at about 50-60 ºC, and then gradually decreased (Fig. 5c and e). In contrast, $C_8H_{12}O_4$ (Fig. 5a) shows two maxima (at ~ 50-60 ºC and ~ 120 ºC), which causes a broader signal. In addition, (in Fig.5a) at T > 120 ºC, the signal intensity stays high. In Figure 5b, d and f, we present the TD-DMA thermograms. Two heating cycles are performed in order to estimate the signal coming from the particles and the signal coming from the background due to the inlet line. Based on the filament resistance, we estimated that the temperature gradually increased up to approximately

600 ºC in a period of ~ 1 minute. In the first heating cycle, the normalized intensity of $C_9H_{14}O_4$ and $C_{10}H_{16}O_6$ (Fig. 5d and f) rapidly increased, reached a maximum and subsequently decreased (sharp peak). As in Fig. 5a, the thermal profile of $C_8H_{12}O_4$ in TD-DMA (Fig. 5b) shows a broadened signal with a multimodal behavior, in which the $C_8H_{12}O_4$ signal at ~ 250 ºC reached background levels. In the second heating cycle (performed immediately afterwards, without particle collection), the normalized intensity remains stable and close to zero. The particle signal is estimated by subtracting the second heating from the first heating.

3.2.1 Positive matrix factorization results

The results of the PMF analysis of the TD-DMA data are shown in Figure 6 which contains the factor mass spectra (Fig. 6a-d), the factor thermograms (Fig. 6e), and the contribution of each factor to the total signal (Fig. 6f). We found that four factors are the best choice to reconstruct the TD-DMA data and to provide the most interpretable results (the residuals are shown in Fig. S7 in the Supplement). We numbered the factors according to their peak desorption temperatures (Fig. 6e). F1 $_{\text{TD-DMA}}$ which desorbs at the very first stages of the heating cycle, includes organic compounds with molecular masses between 150 and 250 Da (M_{av} = 211.6 Da), with a carbon, hydrogen and oxygen average content (CHO_{ac}) of 9.2, 14.6 and 5.4, respectively. F1 $_{\text{TD-DMA}}$ contains mainly compounds in the monomer region (see Fig. S8 in the Supplement). F2 $_{\text{TD-DMA}}$ desorbs right after F1 $_{\text{TD-DMA}}$. The mass average (M_{av}) is 230.7 Da and the CHO_{ac} is 10.0, 16.1 and 5.9. Compounds in the monomer region also contribute to this factor (see Fig. S8 in the Supplement). F3 $_{\text{TD-DMA}}$ shows a clear contribution of both monomers and dimers for the time when the time series shows a broadened peak. CHO_{ac} is 10.8, 16.7 and 5.5 and M_{av} = 234.5 Da. Lastly, F4 $_{\text{TD-DMA}}$ is dominated (~ 60 % of the signal intensity) by a high signal with molecular mass of 172.18 Da, which corresponds to $C_8H_{12}O_4$. This is reflected by lower values of CHO_{ac} and M_{av} compared to the other factors (CHO_{ac} = 8.6, 12.8, and 4.5, M_{av} = 188.2 Da). By looking closer into F4$_{\text{TD-DMA}}$ (Fig. 6d), we observe that some compounds with mass < 200 Da also contribute to this factor. By integrating each factor thermogram (Fig. 6e), we calculated that F1 $_{\text{TD-DMA}}$ and F2 $_{\text{TD-DMA}}$ contribute to ~ 70 % of the total signal while F3 $_{\text{TD-DMA}}$ and F4 $_{\text{TD-DMA}}$ make up ~ 30 % of the total signal as shown in Figure 6f.

On the other hand, we present in Figure 7 the results from applying PMF to the FIGAERO thermal desorption data for a solution with 6 factors. Figure 7a-f contains the factor mass spectra, Fig. 7g the factor thermograms, and Fig. 7h shows the contribution of each factor to the total particle signal (the residuals and the factors expressed in terms of their oxygen content and mass are shown in Figures S9 and S10 in the Supplement, respectively). F1 $_{\text{FIGAERO}}$, F2 $_{\text{FIGAERO}}$ and F3 $_{\text{FIGAERO}}$ (Fig. 7a-c) show a distinct contribution from monomers, and similar mass spectra, but display different thermal profiles (in Fig. 7g). Specifically, F2 $_{\text{FIGAERO}}$ and F3 $_{\text{FIGAERO}}$ exhibit well-defined thermal profiles (~ 15 ºC difference in T_{max}). However, F1 $_{\text{FIGAERO}}$ shows a broader profile with no distinct maximum. We suspect that F1 $_{\text{FIGAERO}}$ can be related to some of the following causes to some extent: a) Limited resolution of the chosen PMF solution at T < 50 ºC, likely to the presence of two neighbouring factors that were not resolved completely; b) interference from volatile material already evaporating at the beginning of the thermogram and, c) adsorption of gaseous compounds. Reason b could be related to the procedure initiating the desorption, where the filter is flushed with N_2 at ambient temperature before starting the heating ramp, which would likely affect the most volatile material. F4 $_{\text{FIGAERO}}$ and F5 $_{\text{FIGAERO}}$ (Fig. 7d and e) show contribution of both monomers and dimers, with a very similar CHO_{ac} and M_{av}. However, they show different thermogram behavior (~ 20 ºC difference for T_{max}, Fig 7g). F6 $_{\text{FIGAERO}}$ shows mainly contributions from compounds with low mass (< 200 Da) and desorbs mainly at the very end of the heating curve. The contribution of each factor to the total signal is shown in Fig 7h.

As mentioned previously, we observed some factors with similar CHO_{ac} and M_{av} but different thermal behavior, possibly due to the presence of isomers. Molecules with the same composition but different structure and functional groups may exhibit different volatilities. In fact, functionality is one of the driving factors that determines volatility (Pankow and Asher, 2008; Wang et al., 2020). The mass spectrometry techniques reported here are not able to determine the molecular

https://doi.org/10.5194/acp-2022-498
Preprint. Discussion started: 26 August 2022

structure. We further note that the factors F4 $_{\text{TD-DMA}}$ and F6 $_{\text{FIGAERO}}$ desorb mainly at the very last stage of the heating curves, although they both have a clear contribution of compounds with mass < 200 Da, and one of lowest oxygen content of all factors (i.e., the lowest degree of oxidation). We suspect that, F4 $_{\text{TD-DMA}}$ (Fig. 6d) and F6 $_{\text{FIGAERO}}$ (Fig. 7g) are comprised primarily of products of thermal decomposition; the heat applied to desorb the particles instead cleaves certain chemical bonds in (larger) molecules before these could desorb. Small compounds are generally expected to desorb before the transmitted thermal energy (i.e., the desorption temperature) is high enough to cause such decomposition. However, F4 $_{\text{TD-DMA}}$ and F6 $_{\text{FIGAERO}}$ thermal profiles also exhibit a small peak at lower temperatures (observed more clearly in Fig. 7g at ~ 40-50 °C), which is likely direct desorption. This may suggest that the low temperature peak stems from monomers desorbing directly, while the broad high temperature peak represents decomposing dimers/oligomers which are then detected at the composition of the corresponding monomers. Previous studies applying PMF analysis to FIGAERO thermal desorption data also observed the presence of one or more factors dominated by thermal decomposition products for α-pinene and sesquiterpene derived SOA (Buchholz et al., 2020; Li et al., 2021). Those studies concluded that thermal decomposition was the main volatilization process at desorption temperatures above 100 °C with differences between the observed SOA types.

By applying PMF analysis to thermal desorption data we observed that often, several factors are needed to explain the behavior of a single ion. One example is shown in the thermal profile of $C_8H_{12}O_4$ for both FIGAERO and TD-DMA (in the Supplement Fig. S11), in which all the PMF factors contribute. Particularly, F4 $_{\text{TD-DMA}}$ and F6 $_{\text{FIGAERO}}$ explain the $C_8H_{12}O_4$ signal at higher temperature. This is consistent with previous observations. Lopez-Hilfiker et al. (2015) reported a significant contribution of thermal decomposition to the detection of $C_8H_{12}O_4$ in the α-pinene ozonolysis system. However, the presence of the other factors suggests that either there are at least 3 isomers with distinguishable volatility, or that there are different thermal decomposition processes occurring at different desorption temperatures which all form $C_8H_{12}O_4$ as a stable product.

3.3 Advantages and disadvantages

Table 2 summarizes some advantages and disadvantages that should be considered when operating the instruments presented here. When measuring particle chemical composition, the time needed for collecting enough particles (mass) should be carefully considered. This fact becomes a challenge when analyzing nanoparticles, since the small particles do not contribute significantly to the overall SOA mass. For instance, for the experiments reported in this work (see Supplementary Fig. S1), the TD-DMA collection time was around 4 hours, the FIGAERO measured in a semicontinuous mode in which the particle collection lasted 15 minutes and was done every 30 minutes during the whole experiment. In contrast, the EESI-TOF measured continuously (every 10 seconds), whereas, for the offline analysis of FILTERS, the particles were collected during the whole experiment of ~ 8 hours. In addition, the EESI-TOF's total particle signal exhibited a good correlation with the mass concentration calculated from the Scanning Mobility Particle Sizer (SMPS) measurements ($r^2 > 0.94$, Fig. S12 in the Supplementary material). Despite the fact that there is a size-dependence on EESI-TOF sensitivity, EESI-TOF sensitivity decreases as the size of the particles increases (Lee et al., 2021b).

EESI-TOF and FIGAERO provide a faster response (every 10 seconds and every 30 minutes, respectively) than the other two methods, and allows a nearly real time monitoring. This is especially convenient when the chemical composition changes continuously (i.e., in complex environments or during oxidative flow reactor or chamber experiments). In contrast, the particle collection periods for TD-DMA and FILTER (offline analysis) were much longer and depended on the particle load and limit of detection. Besides the low time resolution, a main disadvantage of longer collection times is that aerosol aging may occur during that time. This can potentially change the chemical composition and therefore lead to inaccurate aerosol speciation. Several studies have reported positive and negative artifacts caused by adsorption of gases on the collection surfaces, longer sampling periods, and volatilization of organic species either during collection or during storage (Turpin et al., 1994; Subramanian et al., 2004; Kristensen et al., 2016).

https://doi.org/10.5194/acp-2022-498
Preprint. Discussion started: 26 August 2022

The mass spectrometers coupled to TD-DMA and FIGAERO (nitrate CI-APi-TOF and iodide HRToF-CIMS, respectively) can perform gas-phase measurements while the particle collection takes places. EESI-TOF in the dual-configuration can measure both particle-and gas-phase quasi simultaneously. This allows for a direct comparison between gas-and particle-phase. On the other hand, measurements that are size-resolved with respect to the aerosol size distribution (between 10 to 30 nm) are also feasible by the TD-DMA (Wagner et al., 2018). For the experiments presented here, size selective measurements were not performed to maximize the collected mass and to allow the intercomparison with the other methods.

The mass spectrometry techniques presented here (TD-DMA + nitrate CI-APi-TOF, FIGAERO + iodide HRToF-CIMS and Na^+ EESI-TOF) can only identify chemical formulas but with some limitations. Thus, for example, it is not possible for example to provide structural information or identification of isomers. In contrast, the UHPLC-HESI-HRMS offline method has the advantage of being able to distinguish between clusters, molecules, and isomers based on the chromatographic separation. Furthermore, the fragmentation pattern (via MS^2-experiments) can provide hints to interpret the functional groups and can be used for unambiguous compound identification. Hence, UHPLC-HRMS can provide robust analytical insight of the stable compounds.

The thermal desorption methods (TD-DMA and FIGAERO) exhibit significant thermal decomposition of compounds with desorption temperatures above 100 °C. For the EESI this seems to be less of an issue in general but in some specific studies thermal decomposition was found to be relevant (Bell et al., 2021). PMF analysis of the thermal desorption data from the TD-DMA and FIGAERO could separate the contribution of products from thermal decomposition from those directly desorbing. However, even with this method, it is not possible to obtain information about the original compounds decomposing and their true volatility. The observed decomposition temperature can be used as an upper limit for volatility (i.e., their true volatility is lower than that associated with the apparent desorption temperature).

For the FILTER method, the compounds collected on the filter have to be extracted into a liquid phase for the UHPLC separation. The choice of solvents for this extraction will determine which fraction of organic compounds will be analyzed. The water-methanol mixture used in this study will extract polar, hydrophilic compounds similar to the water-soluble organic carbon category. Note that the exposure to water (or other solvents) may lead to chemical reactions, e.g., hydrolysis of (hydro) peroxides. The selective extraction and potential aqueous phase chemistry may explain the smaller number of compounds detected with the FILTER method. However, for the compounds that do get analyzed, a much deeper understanding can be achieved (e.g., separation of isomers).

The ionization technique also plays a role on the final detection. If the ionization technique is not soft enough, this can result in fragmentation and affects the final response in the detection. In principle, the ionization techniques utilized by the instruments reported here are soft, meaning that no significant fragmentation occurs during the detection. Nevertheless, the ionization efficiency is different between the techniques. For example, with the nitrate reagent ion, highly oxygenated species can be better detected, while the ionization techniques used for FIGAERO and EESI-TOF (I^-, and Na^+, respectively) are more sensitive to intermediately oxygenated organic compounds. The UHPLC-HESI-HRMS can be operated in both polarity modes, however, and therefore detect species are either able to donate protons (in the negative mode) or form clusters with protons or sodium (in the positive mode).

The complete characterization of species in the particle-phase in terms of chemical formula and structure represents an analytical challenge. In this sense, the full identification of organic compounds is only possible by combining different techniques.

4. Conclusions

In this study, we presented an overview of four different methods for measuring the chemical composition of ultrafine particles and we described their capabilities to detect organic compounds. Specifically, we reported the particle-phase composition from α-pinene ozonolysis at -50 ºC, -30 ºC and -10 ºC. In all the cases, the highest portion of detected compounds correspond to species with 10 and less than 10 carbon atoms (C_{10}, $C_{<10}$). The EESI-TOF generally detected a higher fraction (compared to the other techniques: TD-DMA, FIGAERO and FILTERS) of compounds with more than 10 carbon atoms ($C_{>10}$). In terms of volatility classes, EESI-TOF detected the higher fraction of ULVOC in all the experiments reported here, especially for those at lower temperatures (-50 ºC and -30 ºC). We presume that several factors can explain these differences, i.e., thermal decomposition of large compounds (for the thermal desorption methods), for which we applied positive matrix factorization on the thermal profiles and suggested a 4-Factor solution for TD-DMA and a 6-Factor solution for the FIGAERO. Specifically, we suspect that $F4_{\text{TD-DMA}}$ and $F6_{\text{FIGAERO}}$ might be related to thermal decomposition to some extent. The PMF factors dominated by direct desorption can be interpreted as volatility classes, characterized by their T_{max} values (the peak in the respective temperature desorption profiles). Nevertheless, further calibration experiments are needed to determine the relation between T_{max} and saturation concentration. With the offline method UHPLC-HESI-HRMS, we were able to verify the presence of isomers (two isomers for $C_8H_{12}O_4$, $C_{10}H_{16}O_3$, $C_{10}H_{16}O_5$, and three isomers for $C_{10}H_{16}O_4$ and $C_{10}H_{16}O_6$), which represents an important advantage over the online methods reported here.

While the methods generally agree on the most important compounds that are found in the nanoparticles, they all have their strengths and shortcomings. A major limit of these methods is that the measurements of the chemical compounds are not quantitative and only rough estimates of the exact contributions of a compound to the overall chemical composition can be made. However, knowing the limitations of each method and using combinations of the available methods can provide deeper insights into the chemical composition and volatility of nanoparticles.

Data availability. Data related to this article are available upon reasonable request to the corresponding authors.

Supplement The supplement related to this article will be available online.

Author contributions.

L. C., M. S., B. L., M. W., S. B., T. M., M. G., Z. B., L. D., J. Du., H. F., X.-C. H., H. L., N. G. A. M., V. M., H. E. M., G. M., R. M., R. L. M., B. M., A. O., T. P., J. P., M. P., A. A. P., B. R., W. S., J. S., P. T., A. T., N. S. U., D. S. W., S. K. W., A. W., W. Y., M. Z.-W., U. B., J. Kir., M. K., K. L., I. E.-H., N. M. D., A. K., and J. Cu. prepared the CLOUD facility and measurement instruments. L. C., M. S., B. L., M. W., S. B., T. M., M. G., A. A., D. M. B., L. D., J. Du., H. F., X.-C. H., H. L., N. G. A. M., V. M., G. M., R. L. M., B. M., J. S., C. T., A. T., N. S. U., D. S. W., S. K. W., M. Z.-W., and J. Kir. collected the data. L. C., M. S., B. L., M. W., M. T., S. B., A. B., S. K. W., and J. Cu. analyzed the data. L. C., M. S., B. L., M. W., M. T., A. B., M. Sim., A. C. W., M. H., D. M. B., L. D., T. P., D. S., R. C. F., A. H., M. K., K. L., D. W., I. E.-H., N. M. D., A. L. V., A. K., and J. Cu. contributed to the scientific discussion and interpretation of the results. L. C., A. B., U. B., R. C. F., and J. Cu. contributed to the writing of the manuscript.

Competing interests. The authors declare that they have no conflict of interest.

Acknowledgments. We thank CERN for providing the CLOUD facility to perform the experiments and the CLOUD community for supporting this study. We especially would like to thank Katja Ivanova, Timo Keber, Frank Malkemper, Robert Sitals, Hanna Elina Manninen, Antti Onnela, and Robert Kristic for their contributions to the experiment.

Financial support. This work was supported by Innovative Training Networks – ITN 400 (CLOUD-Motion H2020-MSCA-ITN-2017 no. 764991 and no. 701647) and by the German Ministry of Science and Education (CLOUD-16, 01LK1601A). European Union's Horizon 2020 research and innovation program through the ATMO-ACCESS Integrating Activity under grant agreement no. 101008004 and, by no. 895875 ("NPF-PANDA"). Deutsche Forschungsgemeinschaft (DFG; German Research Foundation) (grant no. 410009325). US National Science Foundation Award (AGS-1801280, AGS-1801574, AGS-1801897, AGS-1602086, and AGS-18801329). Swiss National Science Foundation (200020_172602 and 20FI20_172622). CERN/FIS-COM/0028/2019, FCT Portuguese national funding agency for science, research and technology. The Jenny and Antti Wihuri Foundation. ACCC Flagship funded by the Academy of Finland grant number 337549, Academy professorship funded by the Academy of Finland (grant no. 302958), Academy of Finland projects no. 325656, 316114, 314798, 325647 and 341349, "Quantifying carbon sink, CarbonSink+ and their interaction with air quality" INAR project funded by Jane and Aatos Erkko Foundation, Jenny and Antti Wihuri Foundation project "Air pollution cocktail in Gigacity", European Research Council (ERC) project ATM-GTP Contract No. 742206, and the Arena for the gap analysis of the existing Arctic Science Co-Operations (AASCO) funded by Prince Albert Foundation Contract No 2859.

References

Bell, D. M., Wu, C., Bertrand, A., Graham, E., Schoonbaert, J., Giannoukos, S., Baltensperger, U., Prevot, A. S. H., Riipinen, I., El Haddad, I., and Mohr, C.: Particle-phase processing of α-pinene NO3 secondary organic aerosol in the dark, Atmos. Chem. Phys. Discuss., 2021, 1-28, 10.5194/acp-2021-379, 2021.

Breitenlechner, M., Fischer, L., Hainer, M., Heinritzi, M., Curtius, J., and Hansel, A.: PTR3: An Instrument for Studying the Lifecycle of Reactive Organic Carbon in the Atmosphere, Analytical Chemistry, 89, 5824-5831, 10.1021/acs.analchem.6b05110, 2017.

Buchholz, A., Ylisirniö, A., Huang, W., Mohr, C., Canagaratna, M., Worsnop, D. R., Schobesberger, S., and Virtanen, A.: Deconvolution of FIGAERO–CIMS thermal desorption profiles using positive matrix factorisation to identify chemical and physical processes during particle evaporation, Atmos. Chem. Phys., 20, 7693-7716, 10.5194/acp-20-7693-2020, 2020.

Bzdek, B. R., Pennington, M. R., and Johnston, M. V.: Single particle chemical analysis of ambient ultrafine aerosol: A review, Journal of Aerosol Science, 52, 109-120, https://doi.org/10.1016/j.jaerosci.2012.05.001, 2012.

Caudillo, L., Rörup, B., Heinritzi, M., Marie, G., Simon, M., Wagner, A. C., Müller, T., Granzin, M., Amorim, A., Ataei, F., Baalbaki, R., Bertozzi, B., Brasseur, Z., Chiu, R., Chu, B., Dada, L., Duplissy, J., Finkenzeller, H., Gonzalez Carracedo, L., He, X. C., Hofbauer, V., Kong, W., Lamkaddam, H., Lee, C. P., Lopez, B., Mahfouz, N. G. A., Makhmutov, V., Manninen, H. E., Marten, R., Massabò, D., Mauldin, R. L., Mentler, B., Molteni, U., Onnela, A., Pfeifer, J., Philippov, M., Piedehierro, A. A., Schervish, M., Scholz, W., Schulze, B., Shen, J., Stolzenburg, D., Stozhkov, Y., Surdu, M., Tauber, C., Tham, Y. J., Tian, P., Tomé, A., Vogt, S., Wang, M., Wang, D. S., Weber, S. K., Welti, A., Yonghong, W., Yusheng, W., Zauner-Wieczorek, M., Baltensperger, U., El Haddad, I., Flagan, R. C., Hansel, A., Höhler, K., Kirkby, J., Kulmala, M., Lehtipalo, K., Möhler, O., Saathoff, H., Volkamer, R., Winkler, P. M., Donahue, N. M., Kürten, A., and Curtius, J.: Chemical composition of nanoparticles from α-pinene nucleation and the influence of isoprene and relative humidity at low temperature, Atmos. Chem. Phys., 21, 17099-17114, 10.5194/acp-21-17099-2021, 2021.

Curtius, J., Sierau, B., Arnold, F., Baumann, R., Busen, R., Schulte, P., and Schumann, U.: First direct sulfuric acid detection in the exhaust plume of a jet aircraft in flight, Geophysical Research Letters, 25, 923-926, https://doi.org/10.1029/98GL00512, 1998.

Donahue, N. M., Epstein, S., Pandis, S. N., and Robinson, A. L.: A two-dimensional volatility basis set: 1. organic-aerosol mixing thermodynamics, Atmospheric Chemistry and Physics, 11, 3303-3318, 2011.

Duplissy, J., Merikanto, J., Franchin, A., Tsagkogeorgas, G., Kangasluoma, J., Wimmer, D., Vuollekoski, H., Schobesberger, S., Lehtipalo, K., Flagan, R. C., Brus, D., Donahue, N. M., Vehkamäki, H., Almeida, J., Amorim, A., Barmet, P., Bianchi, F., Breitenlechner, M., Dunne, E. M., Guida, R., Henschel, H., Junninen, H., Kirkby, J., Kürten, A., Kupc, A., Määttänen, A., Makhmutov, V., Mathot, S., Nieminen, T., Onnela, A., Praplan, A. P., Riccobono, F., Rondo, L., Steiner, G., Tome, A., Walther, H., Baltensperger, U., Carslaw, K. S., Dommen, J., Hansel, A., Petäjä, T., Sipilä, M., Stratmann, F., Vrtala, A., Wagner, P. E., Worsnop, D. R., Curtius, J., and Kulmala, M.: Effect of ions on sulfuric acid-water binary particle formation: 2. Experimental data and comparison with QC-normalized classical nucleation theory, Journal of Geophysical Research: Atmospheres, 121, 1752-1775, 10.1002/2015JD023539, 2016.

Epstein, S. A., Riipinen, I., and Donahue, N. M.: A semiempirical correlation between enthalpy of vaporization and saturation concentration for organic aerosol, Environmental science & technology, 44, 743-748, 2009.

Gonser, S. G., and Held, A.: A chemical analyzer for charged ultrafine particles, Atmos. Meas. Tech., 6, 2339-2348, 10.5194/amt-6-2339-2013, 2013.

Graus, M., Müller, M., and Hansel, A.: High resolution PTR-TOF: Quantification and formula confirmation of VOC in real time, Journal of the American Society for Mass Spectrometry, 21, 1037-1044, 10.1016/j.jasms.2010.02.006, 2010.

Hallquist, M., Wenger, J. C., Baltensperger, U., Rudich, Y., Simpson, D., Claeys, M., Dommen, J., Donahue, N. M., George, C., Goldstein, A. H., Hamilton, J. F., Herrmann, H., Hoffmann, T., Iinuma, Y., Jang, M., Jenkin, M. E., Jimenez, J. L., Kiendler-Scharr, A., Maenhaut, W., McFiggans, G., Mentel, T. F., Monod, A., Prévôt, A. S. H., Seinfeld, J. H., Surratt, J. D., Szmigielski, R., and Wildt, J.: The formation, properties and impact of secondary organic aerosol: current and emerging issues, Atmos. Chem. Phys., 9, 5155-5236, 10.5194/acp-9-5155-2009, 2009.

He, S., Li, L., Duan, H., Naqwi, A., and Hogan, C. J.: Aerosol Analysis via Electrostatic Precipitation-Electrospray Ionization Mass Spectrometry, Analytical Chemistry, 87, 6752-6760, 10.1021/acs.analchem.5b01183, 2015.

Heinritzi, M., Simon, M., Steiner, G., Wagner, A. C., Kürten, A., Hansel, A., and Curtius, J.: Characterization of the mass-dependent transmission efficiency of a CIMS, Atmos. Meas. Tech., 9, 1449-1460, 10.5194/amt-9-1449-2016, 2016.

Horan, A. J., Apsokardu, M. J., and Johnston, M. V.: Droplet Assisted Inlet Ionization for Online Analysis of Airborne Nanoparticles, Analytical Chemistry, 89, 1059-1062, 10.1021/acs.analchem.6b04718, 2017.

Jayne, J. T., Leard, D. C., Zhang, X., Davidovits, P., Smith, K. A., Kolb, C. E., and Worsnop, D. R.: Development of an Aerosol Mass Spectrometer for Size and Composition Analysis of Submicron Particles, Aerosol Science and Technology, 33, 49-70, 10.1080/027868200410840, 2000.

Kirkby, J., Curtius, J., Almeida, J., Dunne, E., Duplissy, J., Ehrhart, S., Franchin, A., Gagné, S., Ickes, L., Kürten, A., Kupc, A., Metzger, A., Riccobono, F., Rondo, L., Schobesberger, S., Tsagkogeorgas, G., Wimmer, D., Amorim, A., Bianchi, F., Breitenlechner, M., David, A., Dommen, J., Downard, A., Ehn, M., Flagan, R. C., Haider, S., Hansel, A., Hauser, D., Jud, W., Junninen, H., Kreissl, F., Kvashin, A., Laaksonen, A., Lehtipalo, K., Lima, J., Lovejoy, E. R., Makhmutov, V., Mathot, S., Mikkilä, J., Minginette, P., Mogo, S., Nieminen, T., Onnela, A., Pereira, P., Petäjä, T., Schnitzhofer, R., Seinfeld, J. H., Sipilä, M., Stozhkov, Y., Stratmann, F., Tomé, A., Vanhanen, J., Viisanen, Y., Vrtala, A., Wagner, P. E., Walther, H., Weingartner, E., Wex, H., Winkler, P. M., Carslaw, K. S., Worsnop, D. R., Baltensperger, U., and Kulmala, M.: Role of sulphuric acid, ammonia and galactic cosmic rays in atmospheric aerosol nucleation, Nature, 476, 429-433, 10.1038/nature10343, 2011.

Kristensen, K., Bilde, M., Aalto, P. P., Petäjä, T., and Glasius, M.: Denuder/filter sampling of organic acids and organosulfates at urban and boreal forest sites: Gas/particle distribution and possible sampling artifacts, Atmospheric Environment, 130, 36-53, https://doi.org/10.1016/j.atmosenv.2015.10.046, 2016.

Kroll, J. H., Donahue, N. M., Jimenez, J. L., Kessler, S. H., Canagaratna, M. R., Wilson, K. R., Altieri, K. E., Mazzoleni, L. R., Wozniak, A. S., Bluhm, H., Mysak, E. R., Smith, J. D., Kolb, C. E., and Worsnop, D. R.: Carbon oxidation state as a metric for describing the chemistry of atmospheric organic aerosol, Nature Chemistry, 3, 133-139, 10.1038/nchem.948, 2011.

Kürten, A., Rondo, L., Ehrhart, S., and Curtius, J.: Performance of a corona ion source for measurement of sulfuric acid by chemical ionization mass spectrometry, Atmos. Meas. Tech., 4, 437-443, 10.5194/amt-4-437-2011, 2011.

Kürten, A., Jokinen, T., Simon, M., Sipilä, M., Sarnela, N., Junninen, H., Adamov, A., Almeida, J., Amorim, A., Bianchi, F., Breitenlechner, M., Dommen, J., Donahue, N. M., Duplissy, J., Ehrhart, S., Flagan, R. C., Franchin, A., Hakala, J., Hansel, A., Heinritzi, M., Hutterli, M., Kangasluoma, J., Kirkby, J., Laaksonen, A., Lehtipalo, K., Leiminger, M., Makhmutov, V., Mathot, S., Onnela, A., Petäjä, T., Praplan, A. P., Riccobono, F., Rissanen, M. P., Rondo, L., Schobesberger, S., Seinfeld, J. H., Steiner, G., Tomé, A., Tröstl, J., Winkler, P. M., Williamson, C., Wimmer, D., Ye, P., Baltensperger, U., Carslaw, K. S., Kulmala, M., Worsnop, D. R., and Curtius, J.: Neutral molecular cluster formation of sulfuric acid–dimethylamine observed in real time under atmospheric conditions, Proceedings of the National Academy of Sciences, 111, 15019-15024, 10.1073/pnas.1404853111, 2014.

Laitinen, T., Hartonen, K., Kulmala, M., and Riekkola, M. L.: Aerosol time-of-flight mass spectrometer for measuring ultrafine aerosol particles, Boreal Environ Res, 14, 539-549, 2009.

Lee, B. H., Lopez-Hilfiker, F. D., Mohr, C., Kurtén, T., Worsnop, D. R., and Thornton, J. A.: An Iodide-Adduct High-Resolution Time-of-Flight Chemical-Ionization Mass Spectrometer: Application to Atmospheric Inorganic and Organic Compounds, Environmental Science & Technology, 48, 6309-6317, 10.1021/es500362a, 2014.

Lee, C. P., Riva, M., Wang, D., Tomaz, S., Li, D., Perrier, S., Slowik, J. G., Bourgain, F., Schmale, J., Prevot, A. S. H., Baltensperger, U., George, C., and El Haddad, I.: Online Aerosol Chemical Characterization by Extractive Electrospray Ionization–Ultrahigh-Resolution Mass Spectrometry (EESI-Orbitrap), Environmental Science & Technology, 54, 3871-3880, 10.1021/acs.est.9b07090, 2020.

Lee, C. P., Surdu, M., Bell, D. M., Dommen, J., Xiao, M., Zhou, X., Baccarini, A., Giannoukos, S., Wehrle, G., Schneider, P. A., Prevot, A. S. H., Slowik, J. G., Lamkaddam, H., Wang, D., Baltensperger, U., and El Haddad, I.: High-Frequency Gaseous and Particulate Chemical Characterization using Extractive Electrospray Ionization Mass Spectrometry (Dual-Phase-EESI-TOF), Atmos. Meas. Tech. Discuss., 2021, 1-21, 10.5194/amt-2021-325, 2021a.

Lee, C. P., Surdu, M., Bell, D. M., Lamkaddam, H., Wang, M., Ataei, F., Hofbauer, V., Lopez, B., Donahue, N. M., Dommen, J., Prevot, A. S. H., Slowik, J. G., Wang, D., Baltensperger, U., and El Haddad, I.: Effects of aerosol size and coating thickness on the molecular detection using extractive electrospray ionization, Atmos. Meas. Tech., 14, 5913-5923, 10.5194/amt-14-5913-2021, 2021b.

Lee, C. P., Surdu, M., Bell, D. M., Dommen, J., Xiao, M., Zhou, X., Baccarini, A., Giannoukos, S., Wehrle, G., Schneider, P. A., Prevot, A. S. H., Slowik, J. G., Lamkaddam, H., Wang, D., Baltensperger, U., and El Haddad, I.: High-frequency gaseous and particulate chemical characterization using extractive electrospray ionization mass spectrometry (Dual-Phase-EESI-TOF), Atmos. Meas. Tech., 15, 3747-3760, 10.5194/amt-15-3747-2022, 2022.

Li, Z., Buchholz, A., Ylisirniö, A., Barreira, L., Hao, L., Schobesberger, S., Yli-Juuti, T., and Virtanen, A.: Evolution of volatility and composition in sesquiterpene-mixed and α-pinene secondary organic aerosol particles during isothermal evaporation, Atmos. Chem. Phys., 21, 18283-18302, 10.5194/acp-21-18283-2021, 2021.

Lopez-Hilfiker, F. D., Mohr, C., Ehn, M., Rubach, F., Kleist, E., Wildt, J., Mentel, T. F., Lutz, A., Hallquist, M., Worsnop, D., and Thornton, J. A.: A novel method for online analysis of gas and particle composition: description and evaluation of a Filter Inlet for Gases and AEROsols (FIGAERO), Atmos. Meas. Tech., 7, 983-1001, 10.5194/amt-7-983-2014, 2014.

Lopez-Hilfiker, F. D., Mohr, C., Ehn, M., Rubach, F., Kleist, E., Wildt, J., Mentel, T. F., Carrasquillo, A. J., Daumit, K. E., Hunter, J. F., Kroll, J. H., Worsnop, D. R., and Thornton, J. A.: Phase partitioning and volatility of secondary organic aerosol components formed from α-pinene ozonolysis and OH oxidation: the importance of accretion products and other low volatility compounds, Atmos. Chem. Phys., 15, 7765-7776, 10.5194/acp-15-7765-2015, 2015.

Lopez-Hilfiker, F. D., Pospisilova, V., Huang, W., Kalberer, M., Mohr, C., Stefenelli, G., Thornton, J. A., Baltensperger, U., Prevot, A. S. H., and Slowik, J. G.: An extractive electrospray ionization time-of-flight mass spectrometer (EESI-TOF) for online measurement of atmospheric aerosol particles, Atmos. Meas. Tech., 12, 4867-4886, 10.5194/amt-12-4867-2019, 2019.

Paatero, P., and Tapper, U.: Positive matrix factorization: A non-negative factor model with optimal utilization of error estimates of data values, Environmetrics, 5, 111-126, 1994.

Pankow, J. F., and Asher, W. E.: SIMPOL. 1: a simple group contribution method for predicting vapor pressures and enthalpies of vaporization of multifunctional organic compounds, Atmospheric Chemistry and Physics, 8, 2773-2796, 2008.

Phares, D. J., and Collier, S.: Direct Collection of Aerosols by Electrostatic Classification for Size-Resolved Chemical Analysis, Aerosol Science and Technology, 44, 173-181, 10.1080/02786820903482914, 2010.

Simon, M., Dada, L., Heinritzi, M., Scholz, W., Stolzenburg, D., Fischer, L., Wagner, A. C., Kürten, A., Rörup, B., He, X. C., Almeida, J., Baalbaki, R., Baccarini, A., Bauer, P. S., Beck, L., Bergen, A., Bianchi, F., Bräkling, S., Brilke, S., Caudillo, L., Chen, D., Chu, B., Dias, A., Draper, D. C., Duplissy, J., El-Haddad, I., Finkenzeller, H., Frege, C., Gonzalez-Carracedo, L., Gordon, H., Granzin, M., Hakala, J., Hofbauer, V., Hoyle, C. R., Kim, C., Kong, W., Lamkaddam, H., Lee, C. P., Lehtipalo, K., Leiminger, M., Mai, H., Manninen, H. E., Marie, G., Marten, R., Mentler, B., Molteni, U., Nichman, L., Nie, W., Ojdanic, A., Onnela, A., Partoll, E., Petäjä, T., Pfeifer, J., Philippov, M., Quéléver, L. L. J., Ranjithkumar, A., Rissanen, M. P., Schallhart, S., Schobesberger, S., Schuchmann, S., Shen, J., Sipilä, M., Steiner, G., Stozhkov, Y., Tauber, C., Tham, Y. J., Tomé, A. R., Vazquez-Pufleau, M., Vogel, A. L., Wagner, R., Wang, M., Wang, D. S., Wang, Y., Weber, S. K., Wu, Y., Xiao, M., Yan, C., Ye, P., Ye, Q., Zauner-Wieczorek, M., Zhou, X., Baltensperger, U., Dommen, J., Flagan, R. C., Hansel, A., Kulmala, M., Volkamer, R., Winkler, P. M., Worsnop, D. R., Donahue, N. M., Kirkby, J., and Curtius, J.: Molecular understanding of new-particle formation from α-pinene between −50 and +25 °C, Atmos. Chem. Phys., 20, 9183-9207, 10.5194/acp-20-9183-2020, 2020.

Stolzenburg, D., Fischer, L., Vogel, A. L., Heinritzi, M., Schervish, M., Simon, M., Wagner, A. C., Dada, L., Ahonen, L. R., Amorim, A., Baccarini, A., Bauer, P. S., Baumgartner, B., Bergen, A., Bianchi, F., Breitenlechner, M., Brilke, S., Buenrostro Mazon, S., Chen, D., Dias, A., Draper, D. C., Duplissy, J., El Haddad, I., Finkenzeller, H., Frege, C., Fuchs, C., Garmash, O., Gordon, H., He, X., Helm, J., Hofbauer, V., Hoyle, C. R., Kim, C., Kirkby, J., Kontkanen, J., Kürten, A., Lampilahti, J., Lawler, M., Lehtipalo, K., Leiminger, M., Mai, H., Mathot, S., Mentler, B., Molteni, U., Nie, W., Nieminen, T., Nowak, J. B., Ojdanic, A., Onnela, A., Passananti, M., Petäjä, T., Quéléver, L. L. J., Rissanen, M. P., Sarnela, N., Schallhart, S., Tauber, C., Tomé, A., Wagner, R., Wang, M., Weitz, L., Wimmer, D., Xiao, M., Yan, C., Ye, P., Zha, Q., Baltensperger, U., Curtius, J., Dommen, J., Flagan, R. C., Kulmala, M., Smith, J. N., Worsnop, D. R., Hansel, A., Donahue, N. M., and Winkler, P. M.: Rapid growth of organic aerosol nanoparticles over a wide tropospheric temperature range, Proceedings of the National Academy of Sciences, 115, 9122-9127, 10.1073/pnas.1807604115, 2018.

Subramanian, R., Khlystov, A. Y., Cabada, J. C., and Robinson, A. L.: Positive and Negative Artifacts in Particulate Organic Carbon Measurements with Denuded and Undenuded Sampler Configurations Special Issue of Aerosol Science and Technology on Findings from the Fine Particulate Matter Supersites Program, Aerosol Science and Technology, 38, 27-48, 10.1080/02786820390229354, 2004.

Surdu, M., Pospisilova, V., Xiao, M., Wang, M., Mentler, B., Simon, M., Stolzenburg, D., Hoyle, C. R., Bell, D. M., Lee, C. P., Lamkaddam, H., Lopez-Hilfiker, F., Ahonen, L. R., Amorim, A., Baccarini, A., Chen, D., Dada, L., Duplissy, J., Finkenzeller, H., He, X.-C., Hofbauer, V., Kim, C., Kürten, A., Kvashnin, A., Lehtipalo, K., Makhmutov, V., Molteni, U., Nie, W., Onnela, A., Petäjä, T., Quéléver, L. L. J., Tauber, C., Tomé, A., Wagner, R., Yan, C., Prevot, A. S. H., Dommen, J., Donahue, N. M., Hansel, A., Curtius, J., Winkler, P. M., Kulmala, M., Volkamer, R., Flagan, R. C., Kirkby, J., Worsnop, D. R., Slowik, J. G., Wang, D. S., Baltensperger, U., and Haddad, I. e.: Molecular characterization of ultrafine particles using extractive electrospray time-of-flight mass spectrometry, Environmental Science: Atmospheres, 1, 434-448, 10.1039/D1EA00050K, 2021.

Turpin, B. J., Huntzicker, J. J., and Hering, S. V.: Investigation of organic aerosol sampling artifacts in the Los Angeles basin, Atmos. Chem. Phys., 28, 3061-3071, 10.1016/1352-2310(94)00133-6, 1994.
, 1994.

Ungeheuer, F., van Pinxteren, D., and Vogel, A. L.: Identification and source attribution of organic compounds in ultrafine particles near Frankfurt International Airport, Atmos. Chem. Phys., 21, 3763-3775, 10.5194/acp-21-3763-2021, 2021.

Voisin, D., Smith, J. N., Sakurai, H., McMurry, P. H., and Eisele, F. L.: Thermal Desorption Chemical Ionization Mass Spectrometer for Ultrafine Particle Chemical Composition, Aerosol Science and Technology, 37, 471-475, 10.1080/02786820300959, 2003.

Wagner, A. C., Bergen, A., Brilke, S., Fuchs, C., Ernst, M., Hoker, J., Heinritzi, M., Simon, M., Bühner, B., and Curtius, J.: Size-resolved online chemical analysis of nanoaerosol particles: a thermal desorption differential mobility analyzer coupled to a chemical ionization time-of-flight mass spectrometer, Atmospheric Measurement Techniques, 11, 5489-5506, 2018.

Wang, M., Chen, D., Xiao, M., Ye, Q., Stolzenburg, D., Hofbauer, V., Ye, P., Vogel, A. L., Mauldin, R. L., Amorim, A., Baccarini, A., Baumgartner, B., Brilke, S., Dada, L., Dias, A., Duplissy, J., Finkenzeller, H., Garmash, O., He, X.-C., Hoyle, C. R., Kim, C., Kvashnin, A., Lehtipalo, K., Fischer, L., Molteni, U., Petäjä, T., Pospisilova, V., Quéléver, L. L. J., Rissanen, M., Simon, M., Tauber, C., Tomé, A., Wagner, A. C., Weitz, L., Volkamer, R., Winkler, P. M., Kirkby, J., Worsnop, D. R., Kulmala, M., Baltensperger, U., Dommen, J., El-Haddad, I., and Donahue, N. M.: Photo-oxidation of Aromatic Hydrocarbons Produces Low-Volatility Organic Compounds, Environmental Science & Technology, 54, 7911-7921, 10.1021/acs.est.0c02100, 2020.

Wang, S., Zordan, C. A., and Johnston, M. V.: Chemical Characterization of Individual, Airborne Sub-10-nm Particles and Molecules, Analytical Chemistry, 78, 1750-1754, 10.1021/ac052243l, 2006.

Ye, Q., Wang, M., Hofbauer, V., Stolzenburg, D., Chen, D., Schervish, M., Vogel, A. L., Mauldin, R. L., Baalbaki, R., Brilke, S., Dada, L., Dias, A., Duplissy, J., El Haddad, I., Finkenzeller, H., Fischer, L., He, X., Kim, C., Kürten, A., Lamkaddam, H., Lee, C. P., Lehtipalo, K., Leiminger, M., Manninen, H. E., Marten, R., Mentler, B., Partoll, E., Petäjä, T., Rissanen, M. P., Schobesberger, S., Schuchmann, S., Simon, M., Tham, Y. J., Vazquez-Pufleau, M., Wagner, A. C., Wang, Y., Wu, Y., Xiao, M., Baltensperger, U., Curtius, J., Flagan, R., Kirkby, j., Kulmala, M., Volkamer, R., Winkler, P. M., Worsnop, D. R., and Donahue, N. M.: Molecular Composition and Volatility of Nucleated Particles from α-Pinene Oxidation between -50 °C and +25 °C, Environmental Science & Technology, 10.1021/acs.est.9b03265, 2019.

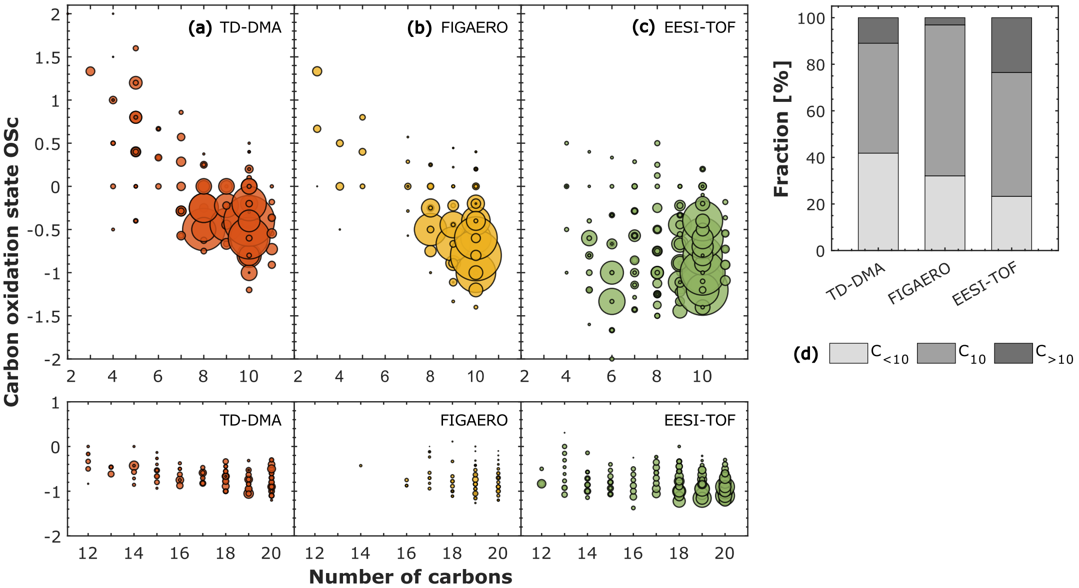

Figure 1. Carbon oxidation state OSc against the number of carbon atoms for α-pinene oxidation products in the particle-phase at -30 ºC and 20 % RH measured by three different techniques. (a) TD-DMA: Thermal Desorption-Differential Mobility Analyzer coupled to a NO_3^- chemical ionization-atmospheric-pressure-interface-time-of-flight mass spectrometer. (b) FIGAERO: Filter Inlet for Gases and AEROsols coupled to an I^- high-resolution time-of-flight chemical-ionization mass spectrometer, and (c) EESI-TOF: Extractive Electrospray Na^+ Ionization time-of-flight mass spectrometer. The level of α-pinene was between 1 and 6 ppbv while the ozone level was ~ 100 ppbv. The carbon oxidation state is calculated as follows: OSc = 2xO:C - H:C. The marker sizes in (a), (b), and (c) represent the intensities normalized by the total signal in each system. (d) Fraction of species in the particle-phase containing less than 10 carbon atoms ($C_{<10}$), 10 carbon atoms (C_{10}), and more than 10 carbon atoms ($C_{>10}$). The fraction was calculated by normalizing the intensities by the total signal in each system.

https://doi.org/10.5194/acp-2022-498
Preprint. Discussion started: 26 August 2022

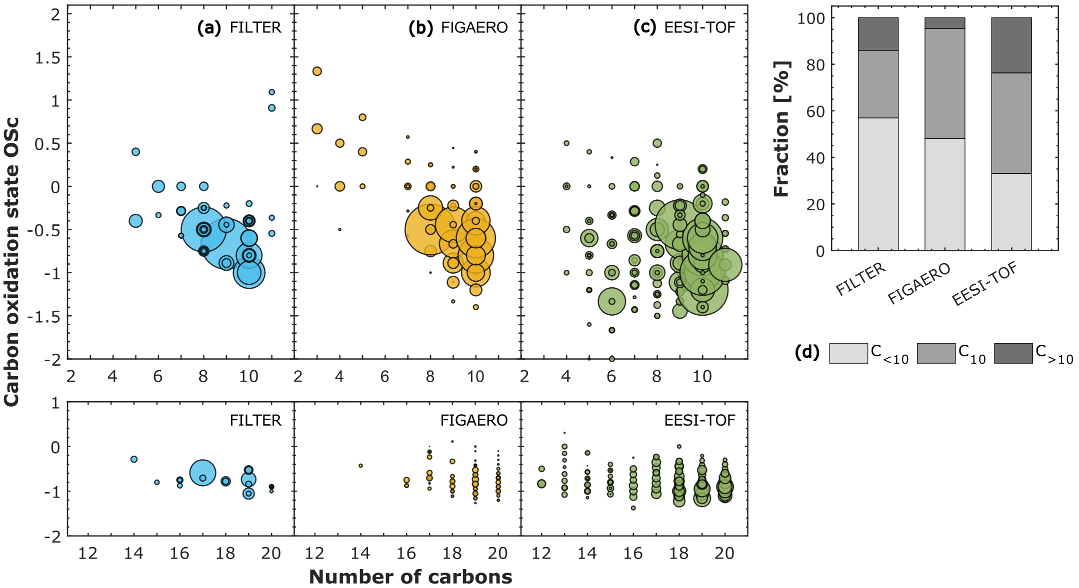

Figure 2. Carbon oxidation state OSc against the number of carbon atoms for α-pinene oxidation products in the particle-phase at -10 ºC and 80 % RH measured by three different techniques. (a) FILTER: Offline analysis of filters using Ultra-high-performance liquid chromatography (UHPLC) and heated electrospray ionization (HESI) coupled to an Orbitrap high-resolution mass spectrometer (HRMS). (b) FIGAERO: Filter Inlet for Gases and AEROsols coupled to an I^- high-resolution time-of-flight chemical-ionization mass spectrometer, and (c) EESI-TOF: Extractive Electrospray Na^+ Ionization time-of-flight mass spectrometer. The level of α-pinene was between 1 and 3 ppbv while the ozone level was ~ 100 ppbv. The carbon oxidation state is calculated as follows: OSc = 2*O:C - H:C. The symbol sizes in (a), (b), and (c) represent the intensities normalized by the total signal in each system. (d) Fraction of species in the particle-phase containing less than 10 carbon atoms ($C_{<10}$), 10 carbon atoms (C_{10}), and more than 10 carbon atoms ($C_{>10}$). The fraction was calculated by normalizing the intensities by the total signal in each system.

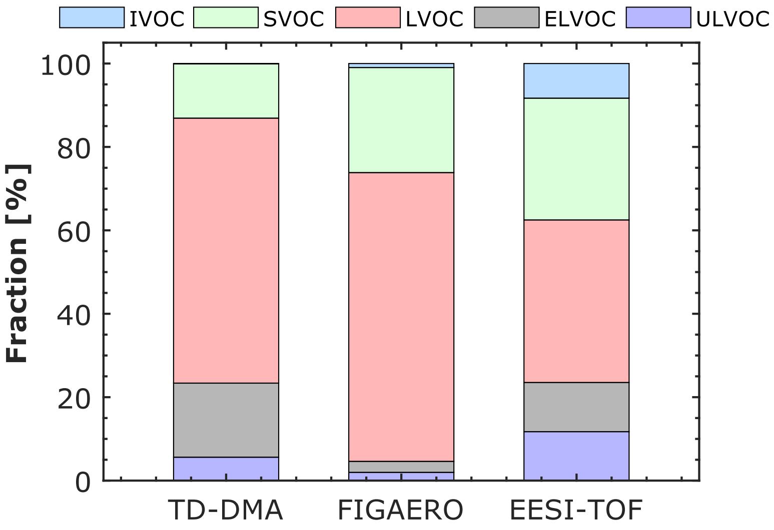

Figure 3. Distribution of volatility classes for α-pinene oxidation products in the particle-phase at -30 °C and 20 % RH measured by three different techniques: (TD-DMA) Thermal Desorption-Differential Mobility Analyzer coupled to a NO_3^- chemical ionization-atmospheric-pressure-interface-time-of-flight mass spectrometer, (FIGAERO) Filter Inlet for Gases and AEROsols coupled to an I^- high-resolution time-of-flight chemical-ionization mass spectrometer, and (EESI-TOF) Extractive Electrospray Na^+ Ionization time-of-flight mass spectrometer. The level of α-pinene was between 1 and 6 ppbv while the ozone level was ~ 100 ppbv. The volatility classes (ULVOC, ELVOC, LVOC, SVOC, IVOC) were defined as in Donahue et al. (2012) and in Schervish and Donahue (2020).

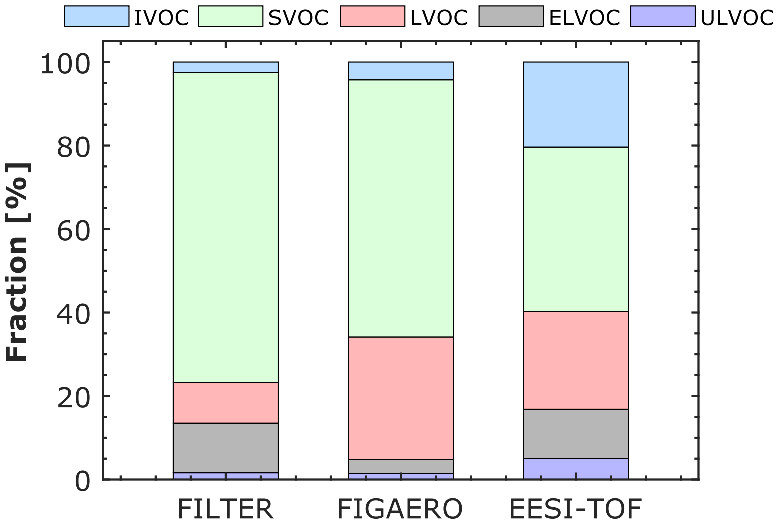

Figure 4. Distribution of volatility classes for α-pinene oxidation products in the particle-phase at -10 °C and 80 % RH measured by three different techniques: (FILTER) Offline analysis of filters using Ultra-high-performance liquid chromatography and heated electrospray ionization coupled to an Orbitrap high-resolution mass spectrometer, (FIGAERO) Filter Inlet for Gases and AEROsols coupled to an I^- high-resolution time-of-flight chemical-ionization mass spectrometer, and (EESI-TOF) Extractive Electrospray Na^+ Ionization time-of-flight mass spectrometer. The level of α-pinene was between 1 and 3 ppbv while the ozone level was ~ 100 ppbv. The volatility classes (ULVOC, ELVOC, LVOC, SVOC, IVOC) were defined as in Donahue et al. (2012) and in Schervish and Donahue (2020).

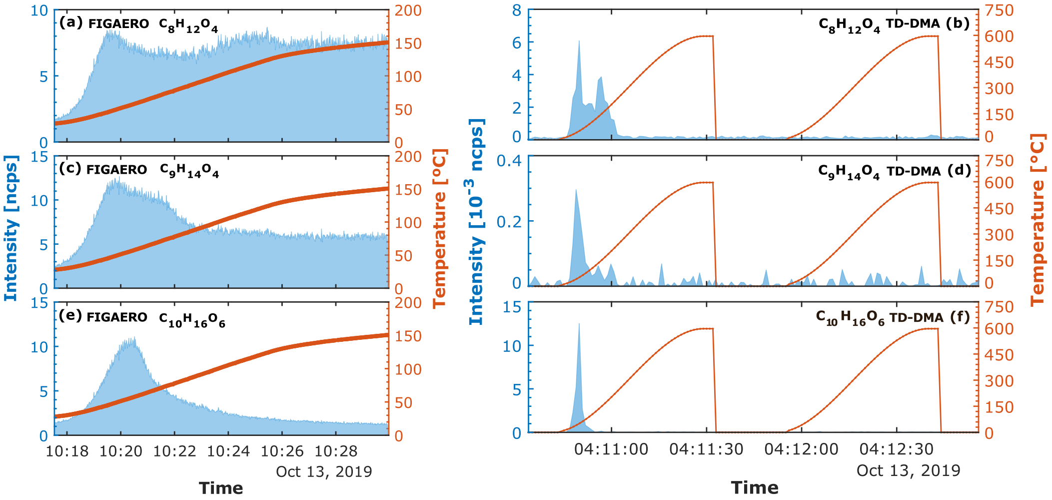

Figure 5. FIGAERO and TD-DMA thermal desorption profiles for three different compounds detected in α-pinene ozonolysis experiment at -30 °C and 20 % RH. (a), (c) and, (e) show FIGAERO thermograms for $C_8H_{12}O_4$, $C_9H_{14}O_4$ and, $C_{10}H_{16}O_6$, respectively. While (b), (d) and, (f) present TD-DMA thermograms for $C_8H_{12}O_4$, $C_9H_{14}O_4$ and, $C_{10}H_{16}O_6$, respectively. FIGAERO and TD-DMA intensities are normalized by the reagent ions and expressed in normalized counts per second (ncps). Both FIGAERO and TD-DMA heating profiles are plotted as a function of temperature. The TD-DMA temperature is an estimate based on the resistance of the filament. For the TD-DMA two heating profiles are needed for determining the particle signal and the background due to the heating of the inlet line.

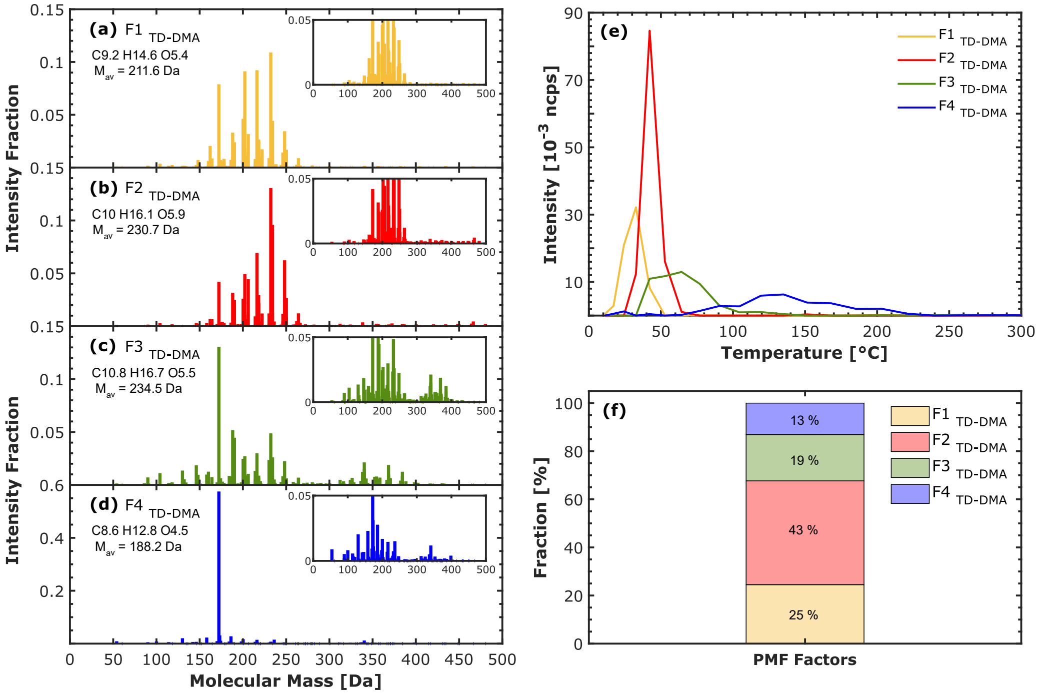

Figure 6. PMF suggested solution on the particle-phase detected by the TD-DMA in α-pinene ozonolysis experiment at -30 °C and 20 % RH. (a), (b), (c) and, (d) Factors mass spectra, (e) Factors thermograms and, (f) Factors fraction. Each factor mass spectrum is normalized and colored according to the order of appearance in the thermogram: F1$_{\text{TD-DMA}}$ (yellow), F2$_{\text{TD-DMA}}$ (red), F3$_{\text{TD-DMA}}$ (green), and F4$_{\text{TD-DMA}}$ (blue). The thermogram (e) is expressed as a function of the temperature, which is an estimation based on the filament resistance. The particle-phase signal has been background corrected.

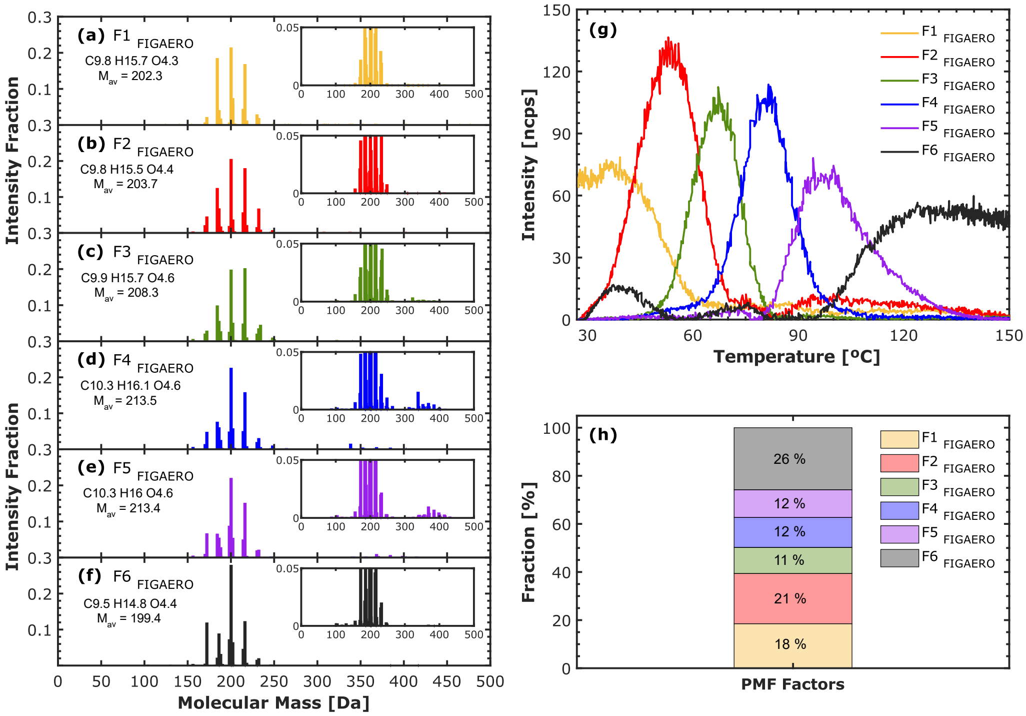

Figure 7. PMF suggested solution on the particle-phase detected by FIGAERO in α-pinene ozonolysis experiment at -30 ºC and 20 % RH. (a), (b), (c), (d), (e) and, (f) Factors mass spectra, (g) Factors thermograms and, (h) Factors fraction. Each factor mass spectrum is normalized and colored according to the order of appearance in the thermogram: F1 FIGAERO (yellow), F2 FIGAERO (red), F3 FIGAERO (green), F4 FIGAERO (blue), F5 FIGAERO (purple) and, F6 FIGAERO (black). The thermogram is expressed as a function of the temperature which causes the desorption. The particle-phase signal has been background corrected.

Table 1. Instruments for measuring particle-phase chemical composition used in the CLOUD chamber experiments.

	TD-DMA + NO_3^- CI-APi-TOF	**FIGAERO + I^- HRToF-CIMS**	**Na^+ EESI-TOF**	**FILTER UHPLC/HESI/HRMS method**
Continuous or discontinuous	semicontinuos	semicontinuos	continuous	discontinuous - offline
Evaporation method	Thermal desorption	Thermal desorption	Extraction solvent - evaporation	Electrospray solvent - evaporation
Phase measured	Gas and Particle [b]	Gas and Particle [b]	Gas and Particle [b]	Particle
Ionization technique	Chemical ionization	Chemical ionization	Electrospray ionization	Electrospray ionization
Reagent ion	$(HNO_3)NO_3$, NO_3^-	I^-, $(H_2O)I^-$	$(NaI)Na^+$, Na^+	NA negative mode
Target substances	Highly oxygenated	Intermediate oxygenated	Intermediate oxygenated	At least O_1 Any chemical stable species and able to donate protons
Is there thermal fragmentation?	Yes	Yes	No	No
Size resolved for this study?	No[a]	No	No	No
Reference	Wagner et al., 2018	Lopez-Hilfiker et al., 2015	Lopez-Hilfiker et al., 2019	Ungeheuer et al., 2020

[a] TD-DMA can measure both size resolved and non-size resolved. For this work it was chosen the non-size resolved in order to maximize the mass collected and to intercompare with the particle-phase instruments, [b] in this work, only the particle-phase measurements are reported, [c] gas-and particle-phase can be measured by using the dual-EESI-TOF configuration.

Table 2. Advantages and drawbacks of four different techniques for measuring the chemical composition of nanoparticles.

Instrument	Advantages	Drawbacks
TD-DMA + NO_3^- CI-APi-TOF	- Size resolved particle collection - Gas-phase can be measured while particle collection, gas and particle intercomparison - Detection immediately after collection	- Resolution might depend on the particle load (collection time ~ 4 hours)* - Thermal fragmentation is possible
FIGAERO + I^- HRToF-CIMS	- Gas-phase can be measure while particle collection, gas and particle intercomparison - Detection immediately after collection - Time resolution 30 min: semicontinuous	- Non-size resolved particle collection - Resolution 30 min: semicontinuous - Thermal fragmentation is possible
Na^+ EESI-TOF	- Continuous measurement, 10 seconds time resolution - Gas-phase can be measure using the dual configuration	- Non-size resolved particle collection - size-dependence sensitivity
FILTER UHPLC-HESI-HRMS method	- Differentiates between clusters and molecules (pre-separation makes sure that the compounds are not fragments) - Identify isomers** using chromatography for separation	- Non-size resolved particle collection - Resolution might depend on the particle load (collection time ~ 8 hours)* - Detection not immediately after collection, first stored - Possible aging, sampling artifacts

950 *Collection period for the experiments reported here for TD-DMA and FILTER. **An assumption about the structure can be expressed by doing complementary experiments.